DETAILED ANALYSIS AND TEST CORRELATION OF A STIFFENED COMPOSITE WING PANEL
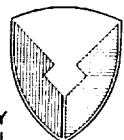
D. Dale Davis, Jr.
Aerostructures Directorate
Aviation Systems Command
Hampton, Virginia

September 1991

DETAILED ANALYSIS AND TEST CORRELATION OF A STIFFENED COMPOSITE WING PANEL

D.D. Davis, Jr.

Abstract

State-of-the-art nonlinear finite element analysis techniques are evaluated by applying them to a realistic aircraft structural component. A wing panel from the V-22 tiltrotor aircraft (shown in Fig. 1) is chosen because it is a typical modern aircraft structural component for which there is experimental data for comparison of results. From blueprints and drawings supplied by Bell Helicopter Textron, Inc., a very detailed finite element model containing 2284 9-node Assumed Natural-Coordinate Strain (ANS) elements was generated. A novel solution strategy which accounts for geometric nonlinearity through the use of corotating element reference frames and nonlinear strain-displacement relations is used to analyze this detailed model. Results from linear analyses using the same finite element model are presented in order to illustrate the advantages and costs of the nonlinear analysis as compared with the more traditional linear analysis. Strain predictions from both the linear and nonlinear stress analyses are shown to compare well with experimental data up through the Design Ultimate Load (DUL) of the panel. However, due to the extreme nonlinear response of the panel, the linear analysis was not accurate at loads above the DUL. The nonlinear analysis more accurately predicted the strain at high values of applied load, and even predicted complicated nonlinear response characteristics, such as load reversals, near the observed failure load of the test panel. In order to understand the failure mechanism of the panel, buckling and first-ply failure analyses were performed. The predicted buckling load was 17% above the observed failure load while first-ply failure analyses indicated significant material damage at and below the observed failure load.
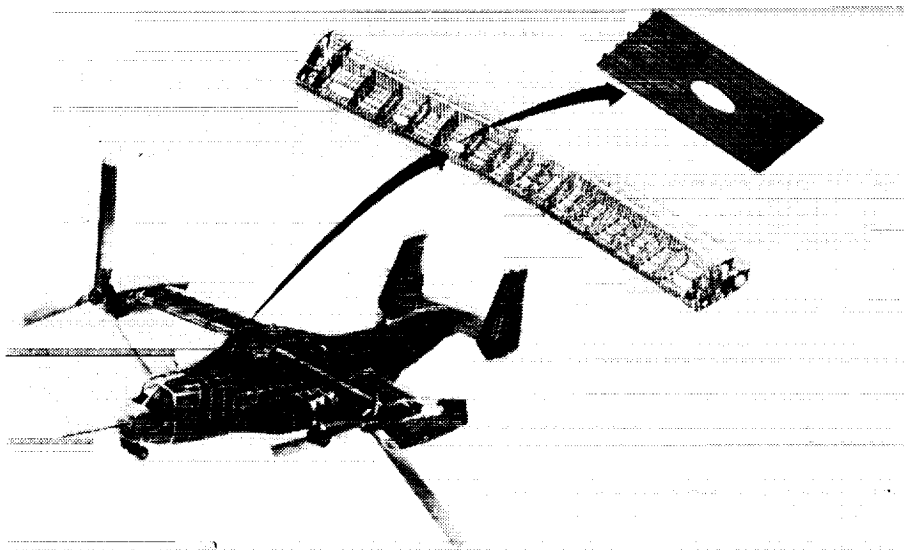
Figure 1. Wing Panel From V-22 Tiltrotor Aircraft

INTRODUCTION

Complex structural systems which incorporate advanced materials and novel configurations require accurate and dependable structural analysis techniques. The finite element method has emerged over the years as the leading analytical tool of the engineer. However, the nonlinear response of very complex structural components has been difficult to predict. Recent advances have made such problems tractable. Advanced finite elements have been developed that are less sensitive to modeling distortion such as warp, taper, skew, and extreme values of aspect ratio than traditional element formulations (Refs. 1-3). Nonlinear solution algorithms have been developed that accurately predict response of highly nonlinear, post-buckled structures (Refs. 4-8). In addition, advancements in computer hardware and software make it possible to predict the response of large structural components whose finite element models require thousands of degrees-of-freedom (Ref. 9).

A major activity is underway at NASA Langley Research Center in structural analysis methods research to provide better analysis tools and techniques for the aerospace industry. With the need for advanced structural analysis methods in mind, a computer code has been developed that serves as a framework for structural analysis methods research. This research code, referred to as the COmputational MEchanics Testbed (COMET), allows new technology to be implemented and compared with other methods in a common software system (Refs. 10-12). COMET currently contains state-of-the-art technology such as improved finite elements, equation solvers, eigensolvers, and solution strategies. There is also ongoing research in constitutive modeling, error detection and control, failure methods, global/local analysis, adaptive mesh refinement, and multiple methods interfacing techniques.

New analysis techniques are often verified using simple textbook problems that have well-known theoretical solutions (Ref. 13). However, even methods that perform well on simple test cases may not be feasible for analysis of realistic structures. The primary purpose of this paper is to examine the performance of recent developments and new techniques by applying them to a complex realistic structure. In particular, a novel finite element formulation and a nonlinear solution algorithm are assessed, and both are described in a later section. A more detailed version of this paper as well as results from mesh convergence and verification studies are presented in another publication[†].

APPROACH

In order to demonstrate the analysis techniques in a manner that is meaningful to industry, a structure was chosen that is typical of a modern aircraft structural component. A panel from the lower wing skin of the V-22 tiltrotor aircraft (see Fig. 1) satisfies this requirement. The panel is made from graphite-epoxy composite material and contains design features such as ply drop-offs, ply interleaves, axial stiffeners, transverse ribs, clips, brackets, and a large central elliptical access hole.

Design blueprints and working drawings of the panel, as well as experimental data, were supplied by Bell Helicopter Textron, Inc. From the blueprints, a very detailed finite element model of the panel was generated. The entire panel, including the clips, brackets, stiffeners, ribs, and load-introduction fixtures, was modeled with shell finite elements. Offsets were used to model the eccentricities caused by the ply drop-offs and interleaves. Boundary conditions were used to simulate the test fixtures and the applied loading. The finite element model is discussed briefly in a later section and in detail in another publication[†].

[†]A NASA Technical Paper entitled "Detailed Analysis Of A Stiffened Composite Wing Panel: Finite Element Modeling, Analysis Techniques, and Test Correlation" by W. J. Stroud, D. D. Davis, Jr.,T. Krishnamurthy, and S. L. McCleary which comprehensively describes the analysis project is currently under preparation.

Many simplified models of the panel, as well as different discretizations of the full model, were analyzed in this study. The results of these preliminary models, although not discussed in this paper, provided great confidence in the element formulation and the nonlinear solution algorithm. Based on results of the preliminary models, the benchmark finite element model was generated. Using this finite element model, linear and nonlinear stress analyses were performed. The analytical results are compared to the strain gage data. The linear and nonlinear results are also compared with each other to illustrate the costs and benefits of the nonlinear analysis.

PANEL DESCRIPTION

General Description

The panel of interest is a large, 35 inches wide by 78 inches long, all-composite panel from the lower wing skin of the V-22 tiltrotor aircraft. Figure 2 is an illustration of the test panel showing the various components and regions of interest. There are five I-shaped stiffeners; the center stiffener is discontinuous due to the presence of the elliptical access hole. The access hole is large enough (12 inches by 21 inches) to permit visual inspection the interior of the wing. This panel is a major structural component having a design ultimate compression load of 334,000 pounds and a design limit compression load of 260,000 pounds. Because of the heavy engines mounted to the ends of the wing, the panel also has specified stiffness requirements. In order to meet the strength and stiffness requirements, several design features were incorporated that greatly complicate the analysis of the panel. The skin beneath the stiffeners is padded up by interleaving 0° plies into the basic skin. The region surrounding the access hole is also padded up, but with ±45° plies instead of 0° plies. The ±45° plies help to transfer the load around the cutout to the adjacent stiffeners. The relatively "soft" skin (90% ±45° plies) along the edge of the cutout minimizes the stress concentration at the free edge where delaminations of the composite material are likely to occur. A complex system of graphite-epoxy and metallic test fixtures are attached to the panel at each end of the access hole to simulate the bulkhead-type transverse ribs of the actual wingbox.
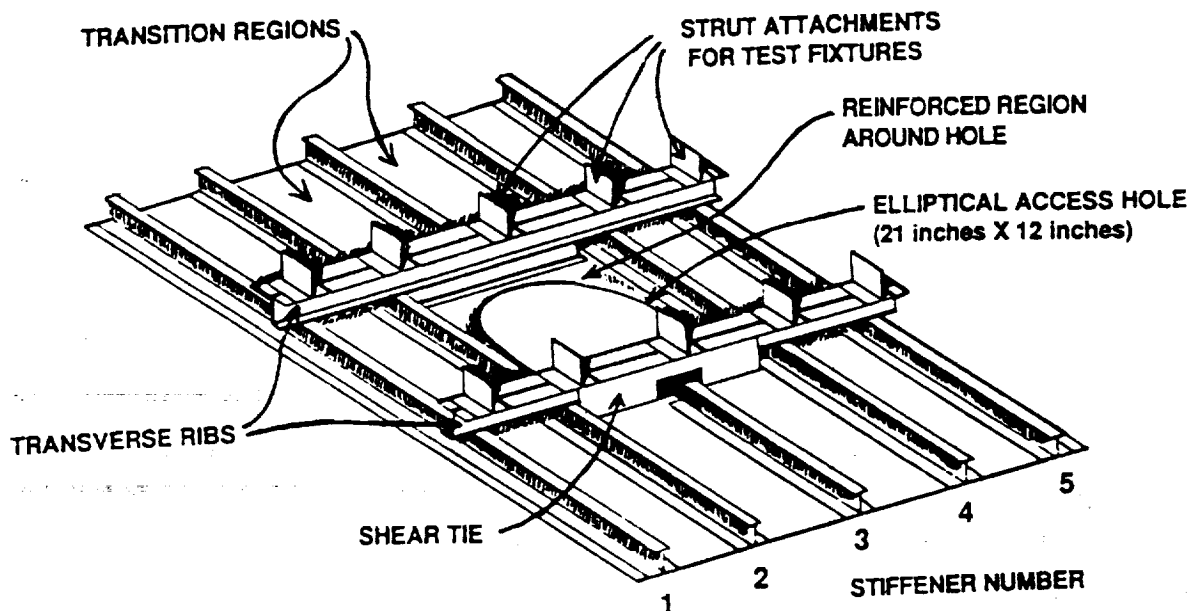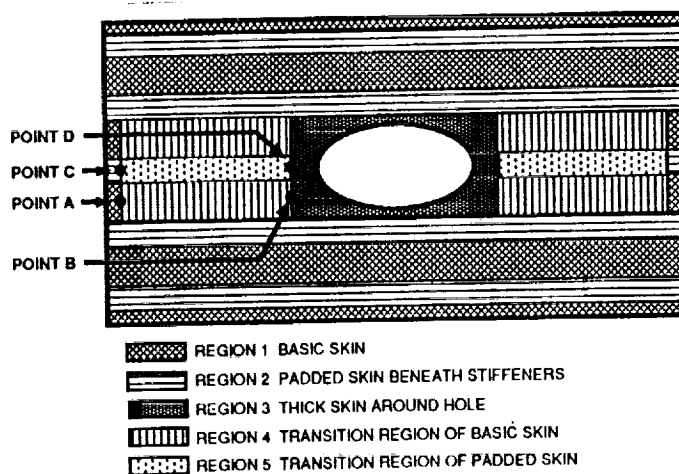

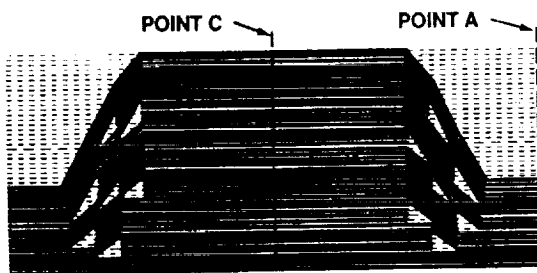Figure 2. Sketch of Key Components of Wing Panel

3

The Skin

The panel skin is very complex due to changes in the stacking sequences caused by numerous ply drop-offs. Basically, the skin can be described in terms of five distinct regions. Figure 3a is a schematic of the panel with the ribs and stiffeners removed and illustrates the five regions of the panel skin. Figures 3b, and 3c are schematics that illustrate the ply stacking sequences for cross-sections AC and AB, respectively, from Figure 3a.
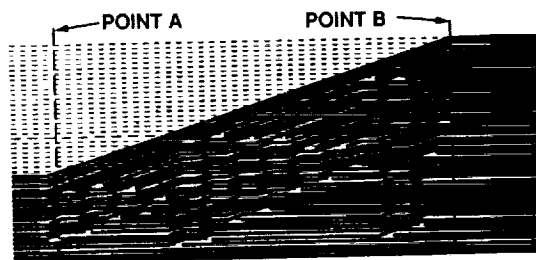
Region 1 is termed the basic skin and consists of 19 plies. Region 2 is the padded region beneath the stiffeners, and is merely the basic skin with 27 $0°$ plies strategically interleaved into it. Figure 4 is a schematic showing a cross-section of the padded region of the basic skin. Region 3, which surrounds the access hole, contains 46 plies and is essentially the basic skin with 27 $±45°$ plies interleaved into it. The layups and thicknesses of Regions 1, 2, and 3 are constant over the regions and are explained in detail in another publication[†]. However, Regions 4 and 5 are transition regions, i.e., regions of the skin where the layup changes point to point due to insertion or replacement of plies. Region 4 is the transition region that transforms Region 1 into Region 3 by interleaving 27 $±45°$ plies. Thus, the thickness of Region 4 gradually increases from 19 plies (at point A) to 46 plies (at point B), as is seen in Fig. 3c. Region 5 is the transition region that transforms Region 2 into Region 3 by replacing 27 of the $0°$ plies of Region 2 with $±45°$ plies. Thus the thickness of Region 5 remains constant (46 plies) while the layup changes from predominantly $0°$ plies at point C to predominantly $±45°$ plies at point D. A more detailed description of the stacking sequences and layups for Regions 4 and 5 is found in another publication[†].

REGION 1 BASIC SKIN
REGION 2 PADDED SKIN BENEATH STIFFENERS
REGION 3 THICK SKIN AROUND HOLE
REGION 4 TRANSITION REGION OF BASIC SKIN
REGION 5 TRANSITION REGION OF PADDED SKIN

a) 5 Sections of Skin

b) Padded Region Beneath Stiffeners

c) Ramp Transition Region

Figure 3. Description of Skin Components

---

† Ibid

The Stiffeners and Ribs

The panel contains five identical stiffeners, four of which (Stiffeners 1, 2, 4, and 5 of Fig. 2) extend the full length of the panel. The center stiffener (Stiffener 3 of Fig. 2), interrupted by the elliptical access hole in the center of the panel, is divided into two 20-inch sections. The construction of the stiffeners consists of five graphite/epoxy components: two identical back-to-back C-channels (15 plies thick), a cap (14 plies thick), and two filler strips. The filler strips are merely 0° plies rolled up to form a plug for the void areas caused by the radius of the corners at the top and bottom of the junction of the back-to-back C-channels.

The caps of the stiffeners are relatively stiff, with approximately 60% 0° plies. The dimensions, stacking sequences, and reference directions for all the components of the stiffeners are given in another publication[†]. The entire stiffener is cocured and then cobonded to the skin with a precured strip of cross-ply cloth between the skin and stiffener. Stiffeners 1, 2, 4, and 5 are cobonded to the top of the padded regions of the basic skin, while Stiffener 3 is cobonded to the top of the transition region (Region 5 of Fig. 3a) along the centerline of the panel.

The bulkhead-type transverse ribs of the actual wing panel are simulated in the test panel by a combination of L-shaped graphite-epoxy channels and metallic test fixtures which are attached to the panel at each end of the access hole. This system is bolted to the caps of Stiffeners 1, 2, 4, and 5, attached to the reinforced skin between Stiffeners 2 and 4 by a graphite-epoxy shear tie, and attached to the end of Stiffener 3 by two L-shaped graphite-epoxy clips. The purpose of the simulated ribs is to provide out-of-plane support for the panel at each end of the discontinuous center stiffener, as do the bulkhead-type ribs of the actual wingbox. Detailed diagrams with dimensions and stacking sequences for the rib system are presented in another publication[†].

TEST DESCRIPTION

Testing of the panel was performed by the Lockheed Georgia Company. The test panel was equipped with 84 uni-axial strain gages and 8 rosettes, for a total requirement of 108 data acquisition channels. The gages were placed in strategic locations over the entire panel, including both sides of the skin, the caps of the stiffeners, and along the edge of the access hole. Figure 4 is a photograph of the panel in the testing machine. The strain gages and strain gage wires are seen attached to the exterior side (skin) of the panel. The stiffener (interior) side of the panel was equipped with a comparable number of strain gages.

The instrumented test panel was aligned in the testing machine, and a compression load was applied to the test panel by lowering the upper crosshead. The horizontal struts shown in Fig. 4 provided out-of-plane support at each end of the access hole. Pins and metallic angle brackets were used to attach the struts to the rib systems. The panel was loaded to failure (405 kips), with strain gage data recorded every 52 kips up to limit load (260 kips), and then every 26 kips until failure. Strain gage locations and the resulting test data were provided to the authors in the form of diagrams, tables, charts, and graphs.

THE ANALYSIS TOOLS

The Software Framework

The analyses were performed using the COmputational MEchanics Testbed (COMET). COMET is an advanced structural analysis code developed at NASA Langley Research Center to provide a framework for structural analysis methods research (Refs. 11-12). This research code contains modules called processors, which are independent FORTRAN executables that perform specific functions. Equation solvers, eigensolvers, mesh generators, element stiffness matrix

---

[†] Ibid

processors, system matrix assemblers, and post-processing packages are all examples of processors. COMET also contains a high-level command language (CLAMP) that, along with the modularity of the processors, provides the user with complete control over the analysis, thus enabling analysis methods research. CLAMP contains many FORTRAN-like functions such as
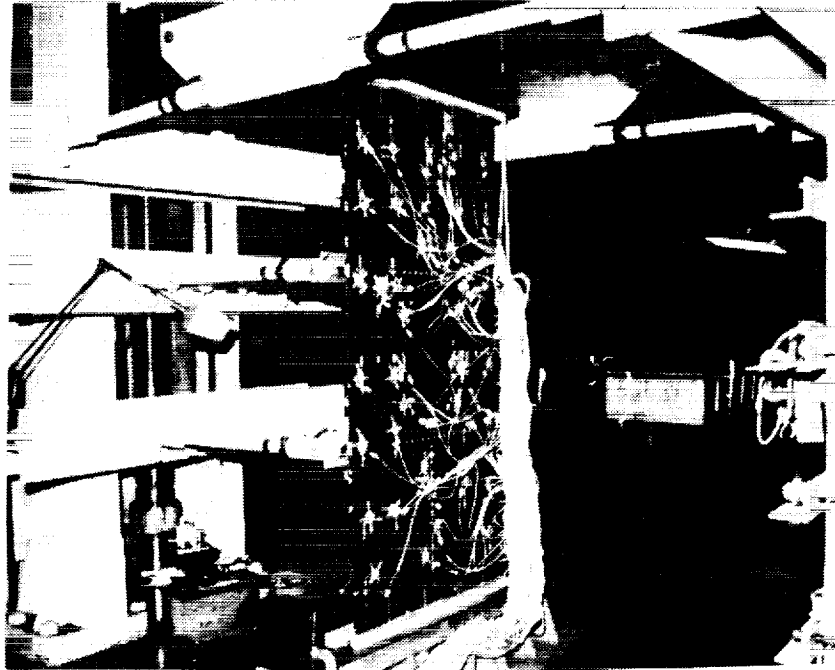

Figure 4. Panel in Testing Machine

logicals, looping, variables, and math functions. By using CLAMP to control the input to and the execution of the processors, very complicated parametric studies can be performed. New techniques can be developed and assessed in the COMET environment without developing all of the supporting software. For example, new equation solvers or finite element formulations can be put into COMET as processors and assessed while using the remainder of the software system and utilities. This allows researchers to concentrate on their areas of expertise without spending large amounts of time generating redundant supporting software.

The Finite Element Formulation

Although there are 10 families of finite elements in COMET, the finite element formulation used in this study is a 9-node assumed natural-coordinate strain (ANS) shell element, denoted within COMET as EX97. The EX97 element has five degrees-of-freedom per node; there is no "drilling" degree-of-freedom. The element is "shear-flexible", i.e., the formulation includes transverse shear stiffness terms. The formulation is based on the assumed strain in the natural (element) coordinate system. A detailed description of the element formulation is given in Refs. 1-3. As compared with other, more traditional formulations, the EX97 proved to be superior, requiring fewer elements for convergence and giving more accurate results when the mesh was distorted[†]. The nonlinear strain-displacement relations of the EX97, when used in conjunction with the corotational capabilities (Ref. 10) of COMET, have given very good results, even in analyses that involved extremely nonlinear, large-rotation, structural response.

[†] Ibid

6

Solution Strategies

Linear Stress Analysis The results for the linear stress analysis were generated by solving the traditional linear system of equations, $F=KU$, where F is the load vector of external applied forces, K is the assembled linear stiffness matrix of the finite element system, and U is the vector of unknown displacements. Based on the solution for the unknown displacements, the stress resultants and strains are then calculated at the element Gauss integration points. The stress resultants and strains are extrapolated to the nodes using the element shape function. In the results section of this paper, the strain results are reported at the nodes, since the location of the certain nodes were made to coincide with the placement of strain gages on the test panel.

Geometrically Nonlinear Stress Analysis Although COMET contains many variations of nonlinear solution techniques, the results from only one such technique are presented herein. The nonlinear solution strategy of interest is a corotational Newton-Raphson algorithm with linearized Crisfield/Riks arc-length control (Ref. 8). The linearized equations of motion are solved iteratively until, based on the convergence criterion, the converged solution is found. Since the tangent stiffness matrix is updated only at the beginning of each new load step, the technique is referred to as a modified Newton-Raphson method. An approach associated with continuation methods for nonlinear problems is based on controlling an equilibrium-path-arc-length parameter. Arc-length control techniques have been developed primarily by Riks (Refs. 14 and 15), Wempner (Ref. 7), and Crisfield (Refs. 4 and 5). The nonlinear solution strategy, the convergence criterion, and the arc-length control strategy are described in detail in Ref. 8.

Bifurcation Buckling The buckling results reported herein were generated by solving the traditional linear structural stability problem, $K\phi_i + \lambda_i K_G \sigma_i = 0$, $i=1,2,...$, where K is the assembled linear elastic stiffness matrix of the system. The assembled geometric stiffness matrix, K_G, dependent only on the state of stress, can be calculated based on the linear or the nonlinear deformed shape of the structure. The i-th eigenvector, ϕ_i, of the equation/solution is the i-th mode shape of the buckled structure. The i-th eigenvalue, λ_i, is the i-th buckling load factor, i.e., the multiple of the applied load that would cause bifurcation of the solution.

First-Ply Failure Analysis For the frst-ply failure analyses, a maximum strain failure criterion was used with the material allowables listed in Table 1. In a first-ply failure analysis, a linear or nonlinear stress analysis is first performed. The state of stress is then calculated for each layer of every element. The layerwise strain components are then compared to the material allowables. If any of the material allowables, by definition the ply has failed. Thus, a first-ply failure analysis is a "snap-shot" analysis, and is based on the state of stress at a given applied load. When a ply "fails", the loads in the ply are not redistributed to adjacent plies and the stiffness of the ply/laminate is not reduced as is done in progressive failure techniques. Because of this, in the literal sense, first-ply failure analysis is only valid up to the point when the first ply fails (hence the term "first-ply failure"). However, with an understanding of these limitations, a rough (though nonconservative) estimate of the damage to the composite material at a given value of structural load can be made.

MATERIAL	STIFFNESS (MSI)			V_{12}	FAILURE STRENGTHS (μ in/in)				
	E_{11}	E_{22}	G_{12}		X_T	X_C	Y_T	Y_C	S
T300/5208	21.0	1.35	0.95	.34	8290	8290	3880	23880	9480
CROSS-PLY CLOTH	3.27	3.27	5.40	.34	3880	23880	3880	23880	9480
ALUMINUM	10.0	10.0	3.54	.30	*	*	*	*	*

* Failure was not considered for the aluminum fixtures.

Table 1. Material Properties Table

FINITE ELEMENT MODEL

Although many simplified preliminary models and perturbations of the benchmark finite element model were studied, only the results for the benchmark model are presented herein. The entire finite element model, close-up views of the edge of the cutout and the edge of a transverse rib, and schematics of the models of the transition region and stiffeners are shown in Fig. 5. Several element types were also studied, but only results for the most robust formulation, the 9-node ANS element, are presented herein. Based on the results of many preliminary models and mesh convergence studies, the relatively coarse mesh around the cutout was determined to be adequate. Another publication[†] contains more detailed descriptions of the preliminary models and results of the convergence studies, the modeling sensitivity studies, and the element performance studies.

The skin, longitudinal stiffeners, and transverse ribs are modeled with the 9-node ANS elements discussed previously. The padded regions and the regions where the stiffener flanges were bonded to the skin were modeled as one contiguous composite finite element through the thickness. Therefore, the appropriate offsets were specified for the elements in order to maintain the eccentricity of the structure. Figure 5 shows a schematic of the stiffener and the corresponding finite element model. The bold lines represent edges of shell elements; the black dots represent the nodes. The eccentricity of the structure is modeled by specifying offsets for the appropriate elements.

The benchmark finite element model contains 2284 elements (all 9-noded ANS elements), 9486 nodes, and 4928 degrees-of-freedom. There are a total of 46 different material section properties. Since the objective was to predict the experimental results, the analysis was performed for only one load case and one constraint case, as is described in the next section.

Composite Material Properties

Due to the complexity of the composite material layups that comprise the panel, only a brief description is included in this section. More details about the stacking sequences for the individual components are given in another publication[†], where the exact material layups of the test panel are illustrated and the corresponding section properties of the finite element model are described.

In COMET, each section property is defined by specifying the number of layers in the section and the material, the angle of orientation, and the thickness for each layer. A laminate analysis utility within COMET (processor LAU) then performs the through-the-thickness integration to calculate the smeared orthotropic laminate properties (the A, B, and D-matrices of Ref. 16). The laminate matrices include the effects of offsets in the shell walls arising from the built-up structure.

The majority of the finite element model of the panel is comprised of multi-layered T300/5208 composite material; the thickness of each layer is .005 inches. A single-layer strip of precured cross-ply cloth was cobonded between the stiffener and the padded skin. It was modeled as one layer in the contiguous layup containing the padded skin, the strip, and the flange of the stiffener. Some parts of the transverse ribs, though actually metallic test fixtures, were modeled with finite elements having the properties of steel. The layerwise material properties are given in Table 1.

The ply drops of the transition region are modeled with four section properties as opposed to modeling all 27 longitudinal ply drops with an individual section property. The layups used for these four sections are the layups from the actual panel at the midpoint of the individual sections. A schematic of the ramp region (from point A to point B of Fig. 3), and the corresponding finite element model are shown in Fig. 5. The appropriate section thicknesses and offsets are also indicated.
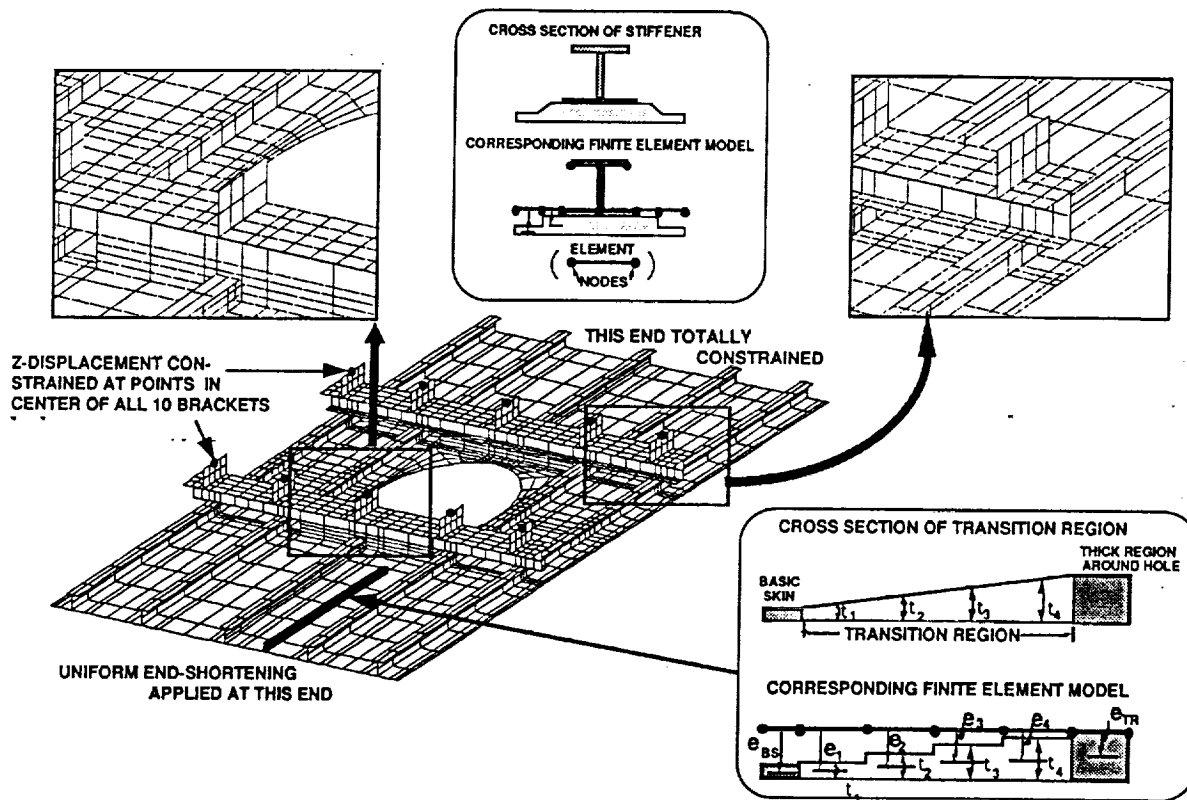

[†] Ibid

Figure 5. The Benchmark Finite Element Model

Loads and Boundary Conditions

To simulate the support struts of the test fixtures, the out-of-plane displacements are constrained to be zero at the midpoint of the top of the fixture brackets (see Fig. 5). At these points, rotations about the global X-axis are constrained and rotations about the global Y-axis are free, to simulate the pins that attach the struts to the rib fixtures. Since the test article is potted at both ends, providing a virtual clamp, all degrees-of-freedom are constrained to be zero at the end $(X = 0)$ of the panel. To simulate the compressive motion of the testing machine crosshead, uniform end-shortening displacement is specified at $X = L$, while all other displacements at $X = L$ are constrained to be zero, as is shown in Fig. 5. The "drilling" degree-of-freedom (the rotational degree-of-freedom whose vector is normal to the plane of the element) is constrained for every appropriate node, since the finite element formulation does not have these "drilling" degrees of freedom.

ANALYSIS RESULTS & TEST CORRELATION

Global Response

Displacements   The load-shortening curves for the linear and nonlinear analyses, as well as the failure load of the test panel, are shown in Figure 6. The global end-shortening response, even in the nonlinear analysis, is very linear through failure. Hence, the panel maintains its stiffness even when heavily-loaded. The nonlinear effects caused by the eccentricity of the discontinuous center stiffener have negligible effect on the global stiffness of the panel, at least up to the failure load.

9

The deformed geometry plots from the linear and nonlinear analyses are shown in Figs. 7a and 7b, respectively. The deformations are scaled by the same relative amount to allow qualitative comparisons to be made. Although the linear and nonlinear analyses indicate approximately the same deformations in the ribs, the out-of-plane deformation at the edge of the cutout is significantly greater in the nonlinear analysis.

As the compressive forces develop in the panel, the skin attempts to expand in the transverse direction due to the Poisson effect. However, the caps of the stiffeners are attached to the relatively stiff transverse ribs, which prevent this Poisson expansion. The result is a complex state of stress in the region between the two transverse ribs. Due to the eccentricity caused by the discontinuous center stiffener, the region around the cutout between the two transverse ribs bends upward, causing an out-of-plane deflection in the positive Z-direction. Because of the complex construction of the test panel, the deformation pattern between ribs is m=1 (one half-wave in the X-direction) and n=2 (two half-waves in the Y-direction) across the panel. Thus, the two stiffeners along the edge of the panel (Stiffeners 1 and 5) are bending in the opposite direction from the two stiffeners adjacent the access hole (Stiffeners 2 and 4).
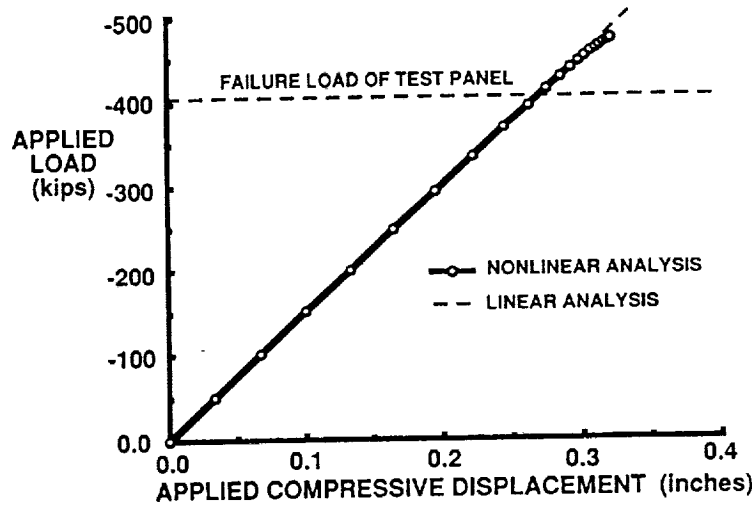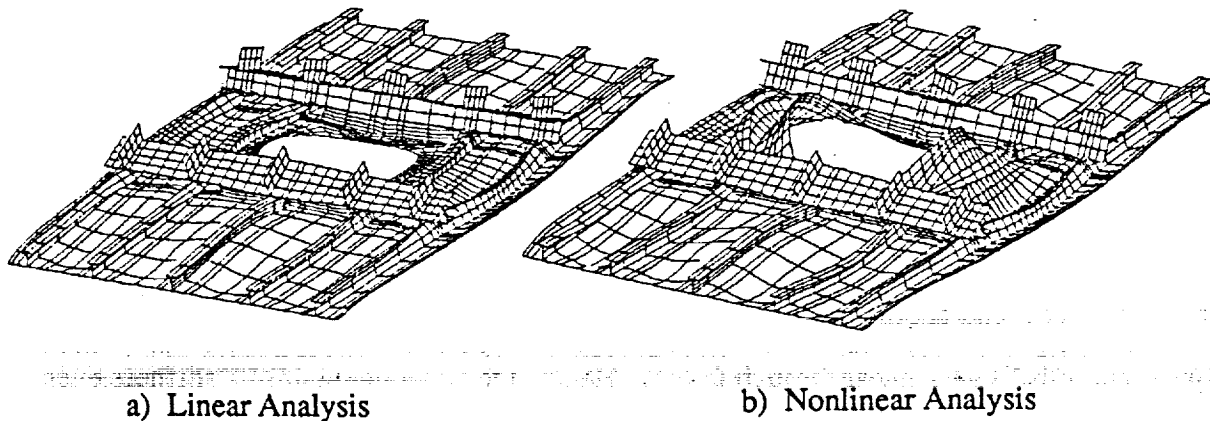

Figure 6. Load Versus End-Shortening

a) Linear Analysis   b) Nonlinear Analysis

Figure 7. Deformed Geometry Plots

10

Local Response

Strains At Panel Midlength   Figure 8 is a plot of the axial strain (ε_x) across the panel midlength for an applied load of 156 kips. The strain gage data are shown as well as strains on the bottom surface of the skin and the top surface of the caps of the stiffeners from the linear and nonlinear analyses. There were 6 strain gages placed along the midlength of the bottom (skin side) of the panel, one at the centerline below each of the Stiffeners 1, 2, 4, and 5, and one at each edge of the cutout, as is indicated in Fig. 8. Four strain gages were placed along the midlength on the stiffener side of the panel, one each at the midlength centerline of the top surface of the caps of Stiffeners 1, 2, 4, and 5. At this value of applied load, both the linear and nonlinear analyses correlated well with test data. Notice the high gradients of strain near the edge of the cutout and across the width of the stiffeners. The high gradients in the stiffeners is an indication of bending in the plane of the panel, as can be seen pictorally in Fig. 7.
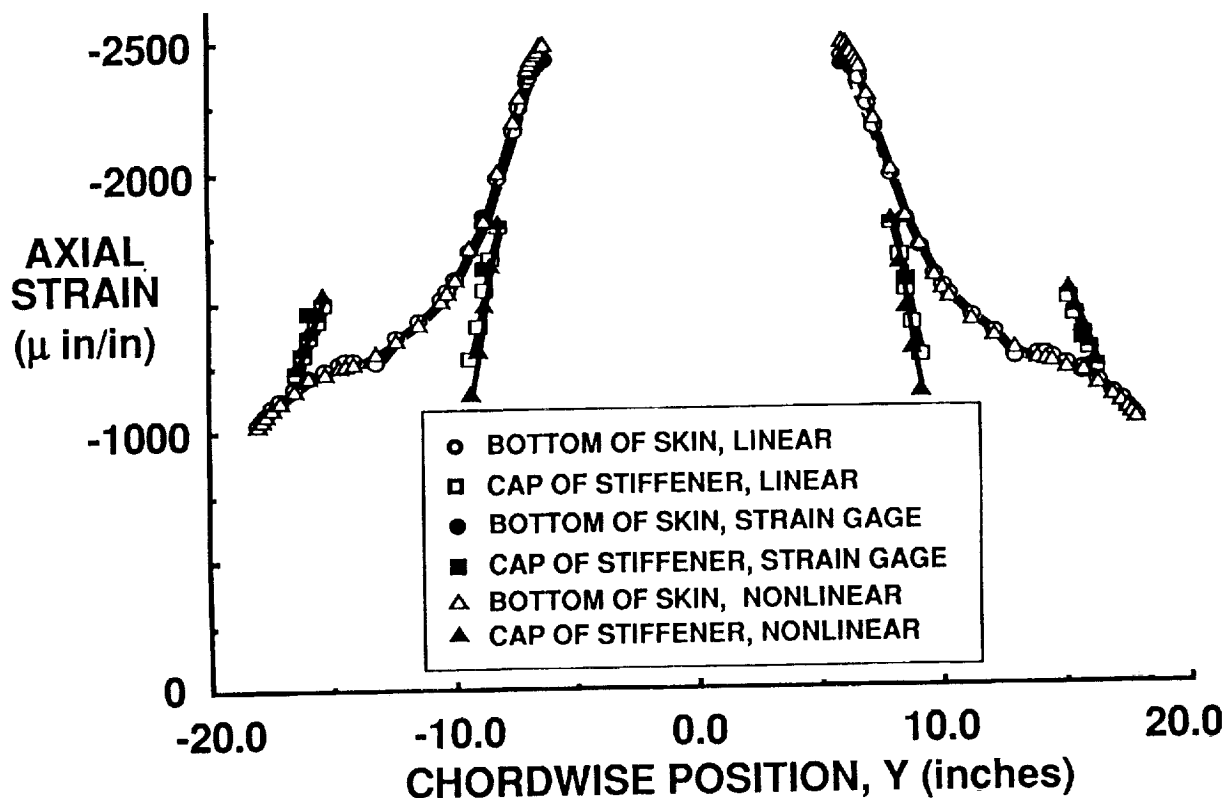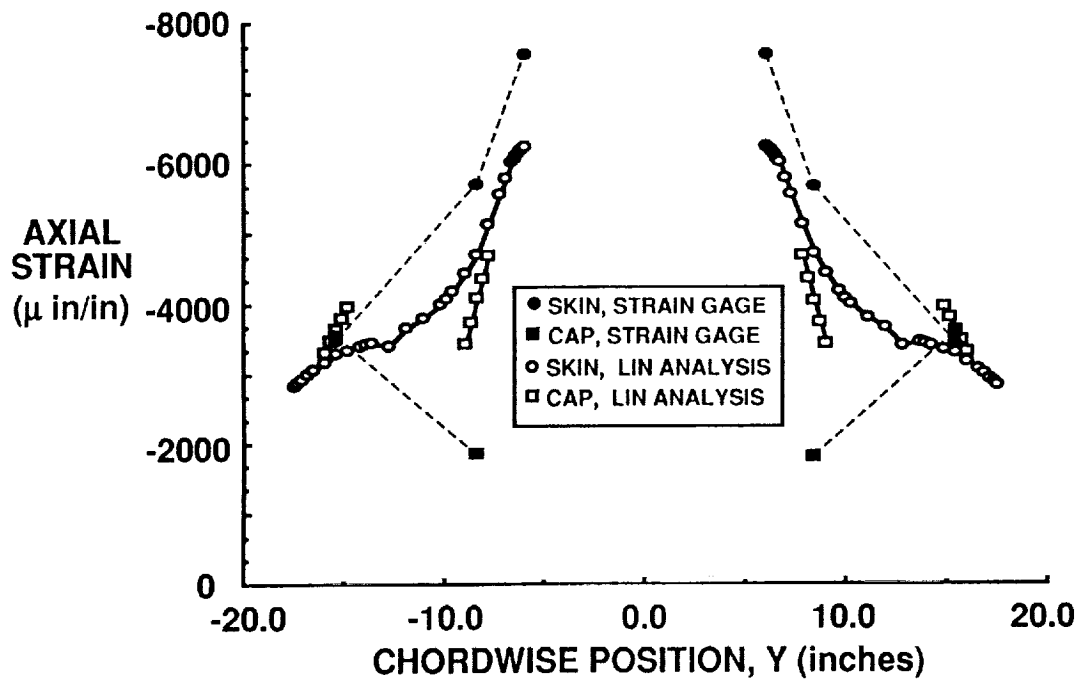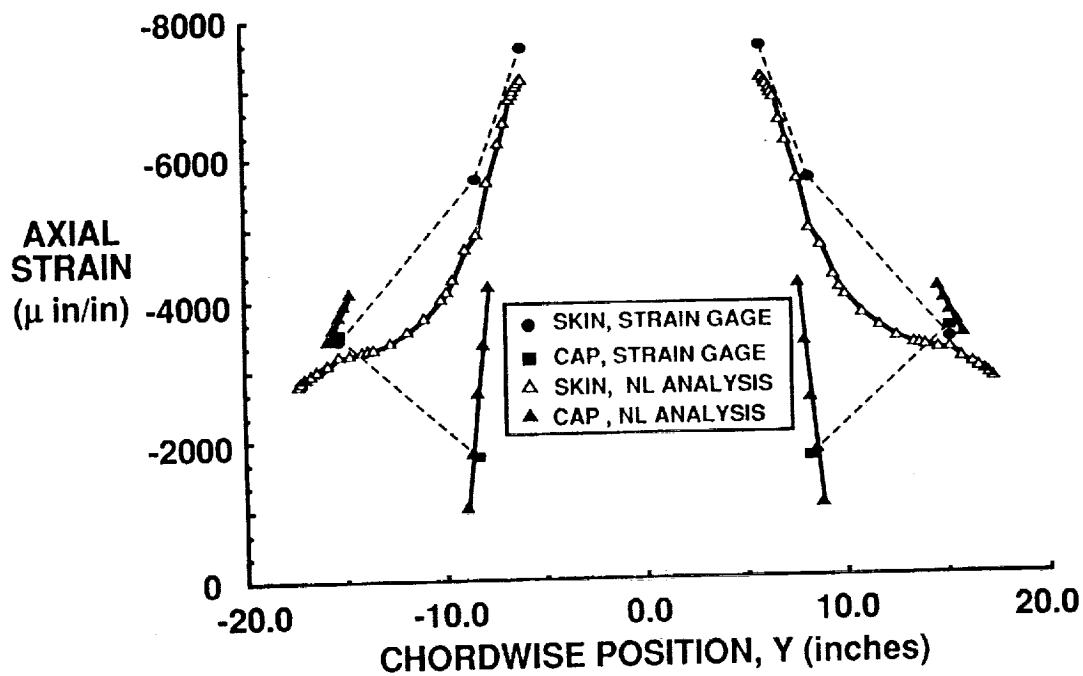

Figure 8. Axial Strain Across Panel Midlength, P=156 kips

Figures 9a and 9b are plots of the axial strain (ε_x) across the panel midlength for an applied load of 396 kips, which is very near the observed failure load of the test panel. Figures 9a and 9b show values for the bottom surface of the skin and the top surface of the caps of the stiffeners from the linear and nonlinear analyses, respectively. At this value of applied load, the linear analysis (Fig. 9a) did not show good correlation with the strain gage data. The linear analysis predicted that the strain on the cap of Stiffeners 2 and 4 would be slightly higher than the strain in Stiffeners 1 and 5. However, the strain gage data indicate that the strain in Stiffeners 2 and 4 is about half of the strain in Stiffeners 1 and 5 at an applied load of 396 kips. The nonlinear results of Fig. 9b much more accurately predict the strain at this load.

11

a) Linear

b) Nonlinear

Figure 9. Axial Strain Across Panel Midlength For Top and Bottom Surfaces of Skin

12

Point Strains as Function of Applied Load   The axial strain (ε_x) is plotted as a function of applied load in Fig. 10. Figure 10a shows results at the midlength of Stiffener 1 for the cap and the bottom of the skin beneath the stiffener. Similarly, Fig. 10b is for Stiffener 2, and Fig. 10c is for the top and bottom surfaces of the skin at the edge of the hole. The open circles represent discrete

a) Top and Bottom of Stiffener 1

b) Top and Bottom of Stiffener 2
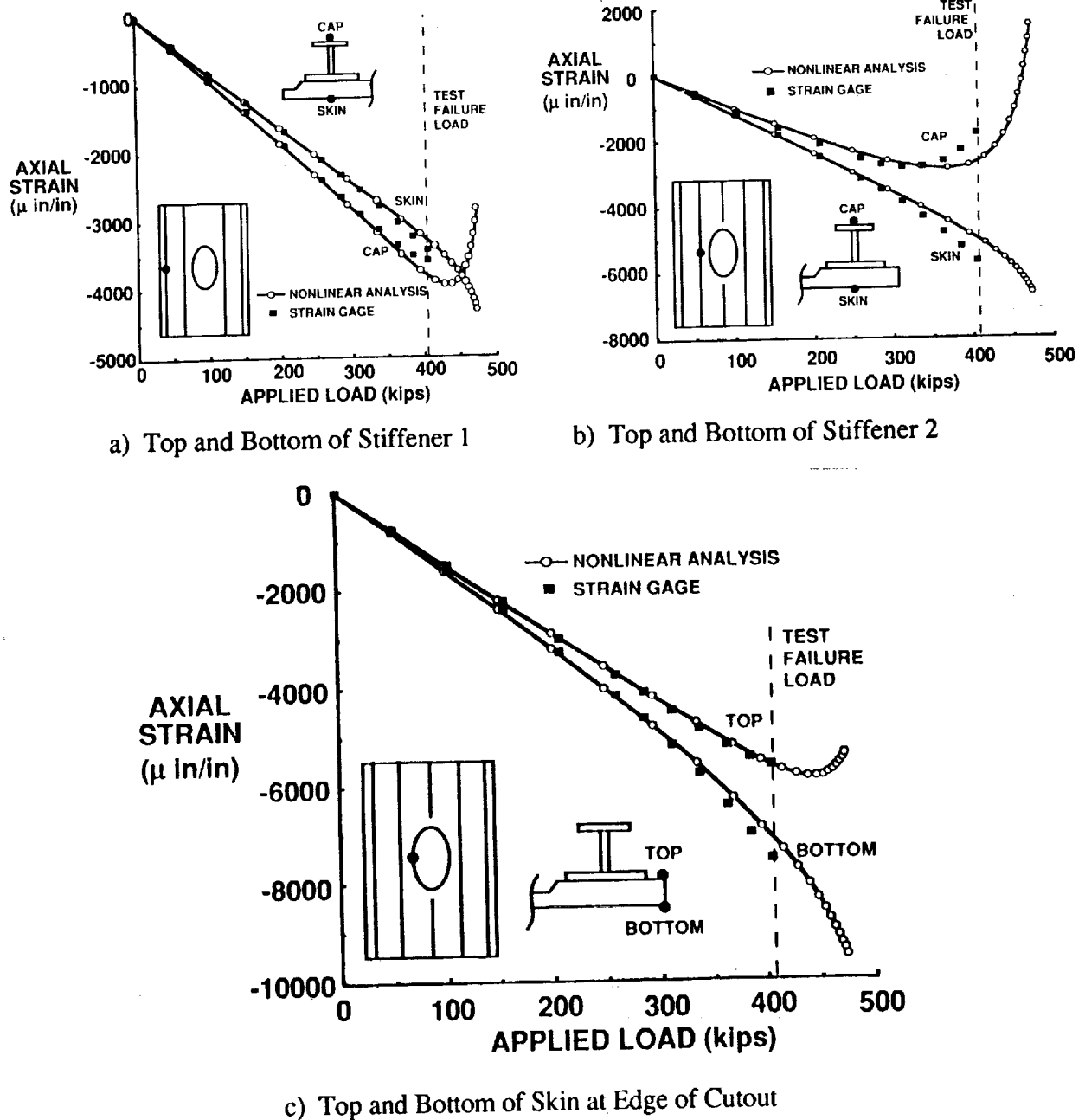
c) Top and Bottom of Skin at Edge of Cutout

Figure 10) Axial Strain as Function of Applied Load

load steps from the nonlinear analysis, the dashed lines represent the extension of the linear path, and the filled symbols represent strain gage data. The vertical line at 405 kips indicates the load at which the test panel failed.The divergence in the strain between the top and bottom surfaces of an element of a structure with increasing applied load is an indication of bending. Stiffener 1 continues to bend, as is indicated by the initial divergence of the strains in Fig. 10a, up to a load of 400 kips. At 400 kips, the stiffener actually begins to unbend, or straighten, as is indicated by the

13

converging strains of Fig. 10a. If the panel had not failed at 405 kips, the nonlinear analysis predicts that, at a load of 453 kips, the stiffener actually would have began bending in the opposite direction. At the same load where Stiffener 1 begins to straighten (400 kips), the bending of Stiffener 2 becomes severe, as can be seen pictorally in Fig. 7b and numerically in Fig. 10b. Stiffener 2 is adjacent to the cutout and is the primary mechanism by which load is redistributed around the cutout. Initially Stiffeners 2 and 4 are bending in opposite directions than Stiffeners 1 and 5, however when the bending of Stiffeners 2 and 4 becomes severe, it actually begins to straighten Stiffeners 1 and 5. The nonlinear analysis predicts that, had the panel not failed at 405 kips, by the time the applied load is 453 kips, all four load-carrying stiffeners would be bending in the same direction. Although the thick skin beneath the stiffeners carry most of the load, the axial strains at the edge of the cutout are the highest in the panel, as is seen in Fig. 10c. These high strains at the edge of the cutout play an important role in the ultimate failure of the panel.

In general, there is excellent agreement between the strain gage data and the stress analysis results. The linear analysis accurately predicted the strains through the DUL of the panel. The nonlinear analysis results slightly under-predict the amount of bending in Stiffeners 1 and 2 at high loads, but the important response characteristics discussed above are correctly identified. The strain at the edge of the cutout, the most critical region in the panel, was accurately predicted all the way through failure of the panel. Although the linear analysis correlated well at the lower loads, the nonlinear analysis was necessary to predict the complicated response of the heavily-loaded panel as it approached the failure load.

EXPLANATION OF FAILURE

Buckling Analysis

As was described previously, linear and nonlinear buckling analyses were performed. The predicted linear buckling load is 495 kips, approximately 17% higher than the observed failure load of the test panel. Contrary to what was expected, the nonlinear buckling load (the buckling load calculated by considering the nonlinear deformed geometry in the geometric stiffness matrix K_G) was not significantly less than the linear buckling load. The critical buckling mode is shown in Fig. 11. Notice that the buckling mode is a simple mode, with all stiffeners bending in the positive Z-direction.
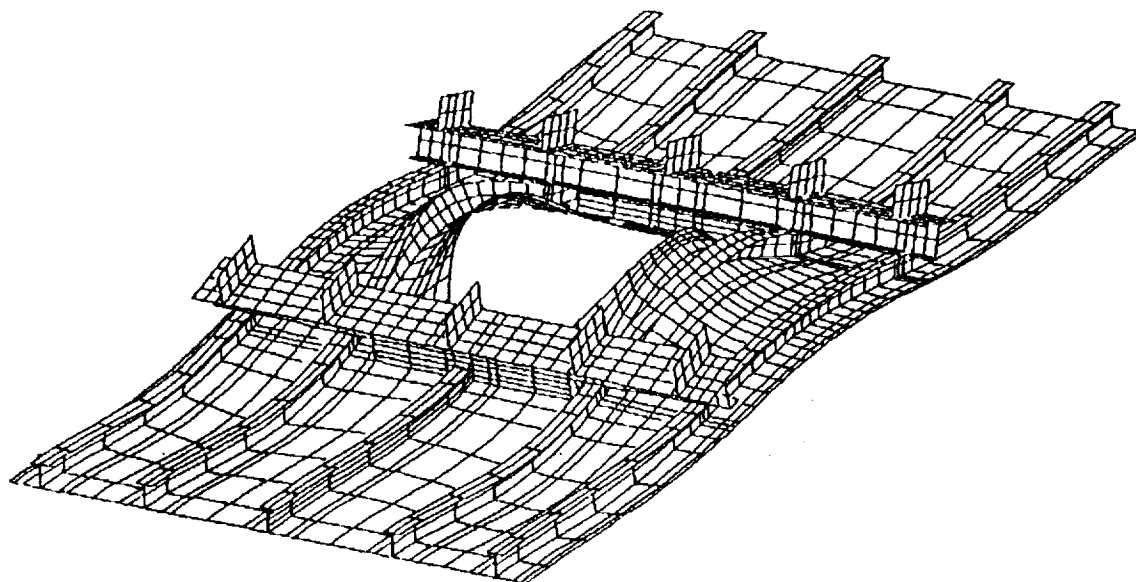

Figure 11. Critical Buckling Mode

14

First-Ply Failure Analysis

Linear and nonlinear first-ply failure analyses were performed as was described previously. In Fig. 12a and 12b, respectively, the elements are shaded according to the percentage of failed plies for the linear and nonlinear analyses for an applied load of 415 kips (the test panel failed at 405 kips). Notice that at this load, both the linear and nonlinear results indicate a significant number of elements with plies that have strain levels exceeding their allowables. The nonlinear analysis predicts more elements with damage, but the linear analysis predicts a much higher percentage of failed plies per element. These differences are attributable to the fact that the nonlinear analysis predicts more bending in the region around the cutout. As the material is compressed and bends, the axial strain on one surface is intensified by the bending and the strain on the other surface is relieved. Therefore, the nonlinear analysis predicts damage at a lower load, or in this case more widespread damage for a given load, and the linear analysis over-predicts the damage as the entire thickness of the element is compressed beyond the compression allowables.
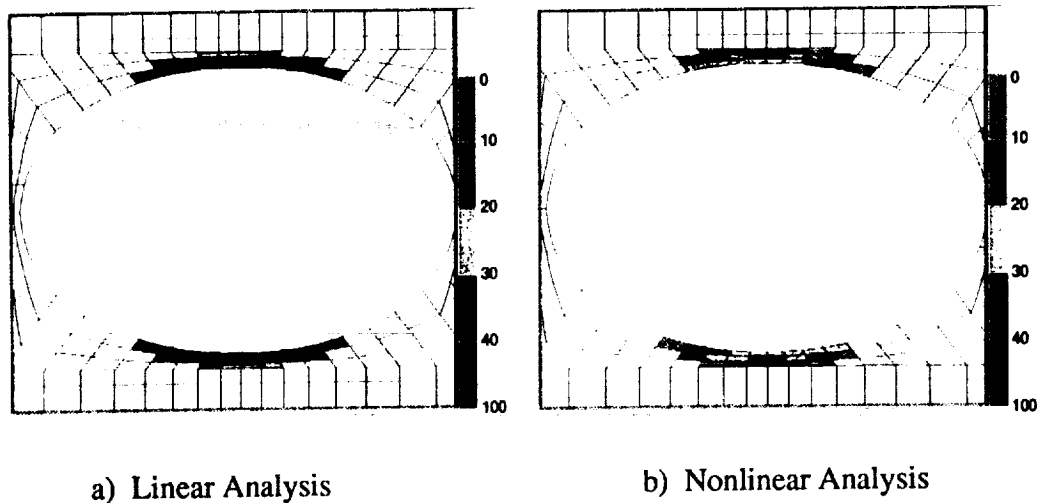

a) Linear Analysis   b) Nonlinear Analysis

Figure 12. Percentage of Failed Plies at 415 kips Applied Load

Discussion of Failure Analysis Results

The first-ply failure results indicate that failure strain allowables were exceeded in a number of plies in the region around the cutout at the observed failure load of the test panel. Because of this and since the linear and nonlinear buckling loads were about 17% above the failure load, it is felt that the panel failed due to excessive strains in the region around the ctuout. The nonlinear analysis predicted the most significant damage to be at the edge of the cutout, a slight angle off of the vertical. The photograph of Fig. 13 shows that the failure zone passed through the edge of the cutout a slight angle off of the vertical. Due to the catastrophic nature of the failure, it is not known that the damage initiated at the edge of the cutout. These conclusions are preliminary at this point because sensitivity studies have not yet been performed to determine the sensitivity of the results to the material failure strain allowables that were used. It is also unknown at this time how sensitive the buckling and nonlinear results are to the imperfections of the stiffeners, because the model assumes that the stiffeners are perfectly straight along the length.

SUMMARY AND CONCLUSIONS

New finite element analysis techniques were evaluated by applying them to a complicated composite wing panel from the V-22 tiltrotor aircraft. A detailed finite element model with a relatively coarse mesh of 9-node elements was generated, and linear and nonlinear stress analyses

were performed. At low values of applied load (up to the design ultimate load of the panel), the linear stress analysis accurately predicted the strains and structural response characteristics of the panel. However, a nonlinear analysis was required to accurately predict the very complicated nonlinear structural response as the applied load approached the failure load of the panel. Calculated surface strains were very accurate as compared with strain gage data, even in critical regions of the panel such as the edge of the cutout and the caps of the stiffeners. Since the first-ply failure analysis indicated damage at the edge of the cutout at the observed failure load of the panel while the calculated buckling load was 17% higher than the failure load, it appears that material damage caused by excessive strain initiated the failure of the panel.
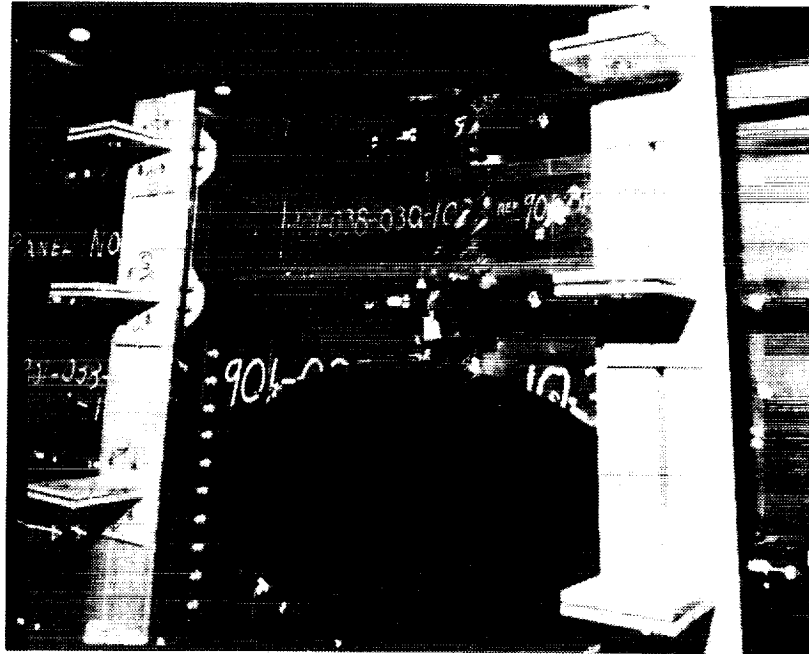

Figure 13. Photograph of Failed Test Panel in Region Around Cutout

ACKNOWLEDGEMENTS

REFERENCES

1. Park, K. C., and Stanley, G. M., A Curved C° Shell Element Based on Assumed Natural-Coordinate Strains, **ASME Journal of Applied Mechanics**, Vol. 108, pp. 278-290, 1986.

2. Stanley, G. M., Continuum-Based Shell Elements, **PhD Dissertation**, Stanford University, Stanford, CA, 1985.

3. Stanley, G. M., Park, K. C., and Hughes, T. J. R., Continuum-Based Resultant Shell Elements, **Finite Element Methods for Plate and Shell Structures, Volume 1:**

---

† Ibid

Element Technology, T. J. R. Hughes and E. Hilton (Editors), Pineridge Press International, Swansea, U. K., pp. 1-45, 1986.

4. Crisfield, M. A., An Arc-Length Method Including Line Searches and Acceleration, **International Journal for Numerical Methods in Engineering**, Vol. 19, pp. 1269-1289, 1982.

5. Crisfield, M. A., A Fast Incremental/Iterative Solution Procedure that Handles Snap-Through, **Computers and Structures**, Vol. 13, pp. 55-62, 1983.

6. Rankin, C. C., and Brogan, F. A., An Element-Independent Corotational Procedure for the Treatment of Large Rotations, **Journal of Pressure Vessel Technology**, Vol. 108, pp. 165-174, 1986.

7. Wempner, G. A., Discrete Approximations Related to Nonlinear Theories of Solids, **International Journal of Solids and Structures**, Vol. 7, pp. 1581-1599, 1971.

8. Stanley, G. M., and Felippa, C. A., Computational Procedures for Postbuckling of Composite Shells, **Proc. of US-Europe Symposium on Finite Element Methods for Nonlinear Problems**, P. G. Bergan, K. J. Bathe, and W. Wunderlich (Editors), Univ. of Trondheim, Norway, pp. 359-385, 1986.

9. Knight, N. F., Jr., Gillian, R. E., McCleary, S. L., Lotts, C. G., Poole, E. L., Overman, A. L., and Macy, S. C., CSM Testbed Development and Large-Scale Structural Applications, NASA TM-4072, 1989.

10. Knight, N. F., Jr., and Stroud, W. J, Computational Structural Mechanics: A New Activity at the NASA Langley Research Center, NASA TM-87612, 1985.

11. Lotts, C. G., Greene, W. H., McCleary, S. L., Knight, N. F., Jr., Paulson, S. S., and Gillian, R. E., Introduction the the Computational Structural Mechanics Testbed, NASA TM-89096, 1987.

12. Stewart, C. B. (Compiler), The Computational Structural Mechanics Testbed User's Manual, NASA TM-100644, 1989.

13. MacNeal, R. H., and Harder, R. L., A Proposed Set of Problems to Test Finite Element Accuracy, **Finite Elements in Analysis and Design**, Vol. 1, pp. 3-20, 1985.

14. Riks, E., On the Numerical Solution of Snapping Problems in the Theory of Elastic Stability, **SUDDAR Report No. 410**, Stanford University, Stanford, CA, 1970.

15. Riks, E., Progress in Collapse Analysis, **ASME Journal of Pressure Vessel Technology**, Vol. 109, pp. 33-41, 1987.

16. Jones, R. M., **Mechanics of Composite Materials**, Scripta Book Company, Washington, DC, 1975.

Report Documentation Page

1. Report No. NASA TM-104154 AVSCOM TR-91-B-015	2. Government Accession No.	3. Recipient's Catalog No.

4. Title and Subtitle Detailed Analysis and Test Correlation of a Stiffened Composite Wing Panel	5. Report Date September 1991
	6. Performing Organization Code

7. Author(s) D. Dale Davis, Jr.	8. Performing Organization Report No.
	10. Work Unit No. 505-63-53

9. Performing Organization Name and Address Aerostructures Directorate U.S. Army-Aviation Systems Command NASA Langley Research Center Hampton, VA 23665-5225	11. Contract or Grant No.
	13. Type of Report and Period Covered Technical Memorandum

12. Sponsoring Agency Name and Address National Aeronautics and Space Administration Washington, DC 20546-0001 and U.S. Army Aviation Systems Command St. Louis, MO 63120-1798	14. Sponsoring Agency Code

15. Supplementary Notes

16. Abstract

State-of-the-art nonlinear finite element analysis techniques are evaluated by applying them to a realistic aircraft structural component. A wing panel from the V-22 tiltrotor aircraft (shown in Fig. 1) is chosen because it is a typical modern aircraft structural component for which there is experimental data for comparison of results. From blueprints and drawings supplied by the Bell Helicopter Textron Corporation, a very detailed finite element model containing 2284 9-node Assumed Natural-Coordinate Strain (ANS) elements was generated. A novel solution strategy which accounts for geometric nonlinearity through the use of corotating element reference frames and nonlinear strain-displacements relations is used to analyze this detailed model. Results from linear analyses using the same finite element model are presented in order to illustrate the advantages and costs of the nonlinear analysis as compared with the more traditional linear analysis. Strain predictions from both the linear and nonlinear stress analyses are shown to compare well with experimental data up through the Design Ultimate Load (DUL) of the panel. However, due to the extreme nonlinear response of the panel, the linear analysis was not accurate at loads above the DUL. The nonlinear analysis more accurately predicted the strain at high values of applied load, and even predicted complicated nonlinear response characteristics, such as load reversals, at the observed failure load of the test panel. In order to understand the failure mechanism of the panel, buckling and first-ply failure analyses were performed. The buckling load was 17% above the observed failure load while first-ply failure analyses indicated significant material damage at and below the observed failure load.

17. Key Words (Suggested by Author(s)) Composite Structures Nonlinear Analysis Finite Element Analysis	18. Distribution Statement Unclassified-Unlimited Subject Category 39		
19. Security Classif. (of this report) Unclassified	20. Security Classif. (of this page) Unclassified	21. No. of pages 18	22. Price A03